UC Riverside

UC Riverside Previously Published Works

Title

Second-harmonic generation of ZnO nanoparticles synthesized by laser ablation of solids in liquids

Permalink

https://escholarship.org/uc/item/4vz57946

Authors

Rocha-Mendoza, I
Camacho-López, S
Luna-Palacios, YY
et al.

Publication Date

2018-02-01

DOI

10.1016/j.optlastec.2017.08.021

Peer reviewed

eScholarship.org Powered by the California Digital Library
University of California

Optics and Laser Technology 99 (2018) 118–123

Contents lists available at ScienceDirect

Optics and Laser Technology

journal homepage: www.elsevier.com/locate/optlastec

Full length article

Second-harmonic generation of ZnO nanoparticles synthesized by laser ablation of solids in liquids

Israel Rocha-Mendoza [a,*], Santiago Camacho-López [a], Yryx Y. Luna-Palacios [b], Yasmín Esqueda-Barrón [a], Miguel A. Camacho-López [c,*], Marco Camacho-López [d], Guillermo Aguilar [e]

[a] Centro de Investigación Científica y de Educación Superior de Ensenada, Carretera Ensenada-Tijuana, No. 3918, Zona Playitas, 22860 Ensenada B.C., Mexico
[b] Posgrado en Ciencia de Materiales, Facultad de Química, Universidad Autónoma del Estado de México, Paseo Colón y Tollocan, Toluca C.P. 50110, Mexico
[c] Laboratorio de Fotomedicina, Biofotónica y Espectroscopía Láser de Pulsos Ultracortos, Facultad de Medicina, Universidad Autónoma del Estado de México, Jesús Carranza y Paseo Tollocan s/n, Toluca C.P. 50120, Mexico
[d] Laboratorio de Investigación y Desarrollo de Materiales Avanzados, Facultad de Química, Universidad Autónoma del Estado de México, Campus Rosedal, Km 14.5 Carretera Toluca-Atlacomulco, San Cayetano de Morelos, Toluca C.P. 50925, Mexico
[e] University of California, Riverside, Department of Mechanical Engineering, 900 University Avenue, Riverside, CA 92521, United States

ARTICLE INFO

Article history:
Received 4 April 2017
Received in revised form 10 June 2017
Accepted 21 August 2017
Available online 12 September 2017

Keywords:
ZnO nanoparticles
Second harmonic generation
Laser ablation of solid in liquids
NLO microscopy
Nanoparticle synthesis

ABSTRACT

We report the synthesis of small zinc oxide nanoparticles (ZnO NPs) based colloidal suspensions and the study of second-harmonic generation from aggregated ZnO NPs deposited on glass substrates. The colloidal suspensions were obtained using the laser ablation of solids in liquids technique, ablating a Zn solid target immersed in acetone as the liquid medium, with ns-laser pulses (1064 nm) of a Nd-YAG laser. The per pulse laser fluence, the laser repetition rate frequency and the ablation time were kept constant. The absorption evolution of the obtained suspensions was optically characterized through absorption spectroscopy until stabilization. Raman spectroscopy, SEM and HRTEM were used to provide evidence of the ZnO NPs structure. HRTEM results showed that 5–8 nm spheroids ZnO NPs were obtained. Strong second-harmonic signal is obtained from random ZnO monocrystalline NPs and from aggregated ZnO NPs, suggesting that the high efficiency of the nonlinear process may not depend on the NPs size or aggregation state.

© 2017 Elsevier Ltd. All rights reserved.

1. Introduction

Highly efficient nonlinear optical properties found in ZnO nanostructures are very attractive as an optical characterization tool and to be used as bio-markers for optical nonlinear imaging [1–3]. For the latter case, second-harmonic generation (SHG), rather than two-photon excitation of fluorescence (TPEF) of ZnO nanoparticles (NPs) is particularly interesting because the SHG process do not cause thermal dissipation in cells, permitting longer time emission without photo-bleaching effects, and the phase matching condition is absent as long as the NPs size is smaller than the excitation wavelength of light, allowing an omnidirectional emission [2] which is useful for transmission and reflection tracking of the SHG signal.

SHG from ZnO has been widely investigated on bulk powders [1], colloidal solutions [2–4], nanowires [5], nanoparticles [2,6,7], from films containing different ZnO grain sizes [8] and nanocomposite films [9], but mostly for nanostructures larger than 20 nm. Controlling the size and/or morphology of ZnO NPs is fundamental to control their second- and third-order nonlinear optical properties [2,3,8,9]. Both the size and the morphology of ZnO NPs are continuously improved with the improvement of the NPs synthesis techniques and, essentially, smaller NPs with determined shape can be fabricated in a controlled way [10,11]. Therefore, recent studies to characterize the nonlinear optical properties of samples containing smaller ZnO NPs are found elsewhere [12]. In this work, we characterize the SHG signal from ZnO NPs of 5–8 nm deposited on glass substrates forming micro-sized structures containing nanoparticle aggregates. Studying the SHG signal of the NPs deposited on substrates rather than in solution is fundamental for biomarking purposes.

The second-order optical nonlinearity of ZnO is originated intrinsically from its crystalline structure, with ZnO crystalizing preferably in the wurtzite-type structure with a hexagonal crystal lattice belonging to the noncentrosymmetric point group 6 mm and space group P63mc. ZnO has large second-order nonlinear

* Corresponding authors.
E-mail addresses: irocha@cicese.mx (I. Rocha-Mendoza), macamachol@uaemex.mx (M.A. Camacho-López).

http://dx.doi.org/10.1016/j.optlastec.2017.08.021
0030-3992/© 2017 Elsevier Ltd. All rights reserved.

coefficients (d_{33} = −5.86 pm/V, d_{31} = 1.76 pm/V and d_{15} = 1.93 pm/V) [13], therefore, the second harmonic generation process is essentially allowed in the electric-dipole approximation away from exciton resonances [14]. When ZnO is synthesized as microcrystalline thin films containing nanostructures, the value of the nonlinear coefficients are 14 times larger than in bulk ZnO and can be resonantly increased as the energy of the SHG frequency approaches the ZnO band gap [4,5,13,14]. These enhanced coefficient values are comparable to the ones found in typical optical crystals ($LiNbO_3$, $LiTaO_3$ and KTP) used for efficient frequency doubling experiments and that is what it makes the SHG process in ZnO nanostructures being observable even to the naked eye.

Several methods for the production of ZnO nanoparticles are found in literature such as hydrothermal methods, electrochemical depositions, sol–gel, chemical vapor deposition, thermal decomposition, combustion methods, chemical-thermal synthesis, anodization, co-precipitation, and electrophoretic deposition [15]. However, many of these methods are inefficient and expensive and, when using chemical synthesis methods, those can produce chemical residuals, which are harmful and toxic for biomedical applications.

The Laser Ablation of Solids in Liquids (LASL) is an experimentally simple, low cost and clean method of synthesis, where it is possible to use organic solvents as the liquid media obtaining nanostructures of very high purity, since there is no need of stabilizing molecules or ligands [16]. This technique has successfully demonstrated the synthesis of ZnO in solution [10,17,18] and zinc peroxide (ZnO_2) nanoparticles [18]. By using the LASL technique it is possible to control the size and morphology of the ZnO NPs through the ablation conditions [10,11]. The ZnO NPs show different physical and chemical properties depending upon their morphology, size and number of defects [17,19]. Furthermore, it has been demonstrated that relatively more stable colloidal nanoparticles solutions are obtained when using the LASL technique [11,16,20–22].

Therefore, the LASL technique results ideal to produce ZnO NPs in a controlled manner and then study their nonlinear optical properties. To the best of our knowledge, no studies characterizing the nonlinear optical properties of ZnO NPs synthesized by LASL has been performed thus far. In this context, the aim of this paper is twofold: firstly, to use the LASL technique as a simple and versatile synthesis route to obtain 5–8 nm ZnO NPs in a controlled manner; secondly, to characterize the nanoparticles SHG response when they are deposited on glass substrates and find its correlation with the ZnO nanostructure. To obtain the ZnO NPs, the ablation of a Zn target immersed in acetone was performed at fixed laser fluence and ablation time. The SHG signal characterization of ZnO NPs was performed using nonlinear SHG microscopy.

2. Experimental

2.1. Synthesis of the ZnO NPs colloidal solutions

The colloidal suspensions of ZnO NPs were synthesized by using a Zn target and acetone as liquid medium (Sigma–Aldrich, Co.). The experimental set up used in the laser ablation experiments is shown in Fig. 1. Nanosecond (ns) laser pulses (7 ± 2 ns pulse duration) from a Nd:YAG laser (Minilite II, Continuum) were used to ablate the Zn target (a disk of 2.54 cm × 0.375 cm, 99.999% pure, Kurt J. Lesker Co.). The laser was operated in its fundamental emission wavelength (1064 nm) at 15 Hz repetition rate. A convex lens of 13.5 cm focal length (L1) is used. Both, the per pulse laser fluence (22 J/cm^2) and the ablation time (10 min) were fixed during the synthesis.

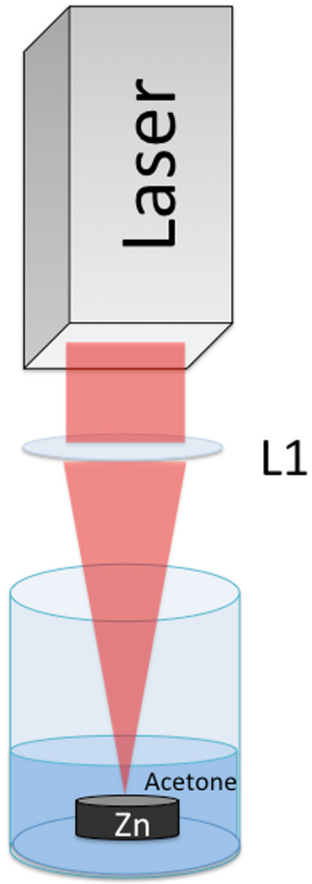

Fig. 1. Experimental set up for LASL experiments. Nanosecond laser pulses are focused to a Zn target, immersed in acetone, to produce ablation. A convex lens of 13.5 cm focal length (L1) is used.

2.2. Sample characterization

2.2.1. UV–Vis characterization

The optical absorption spectra of the colloidal suspensions were taken on a daily basis after the NPs synthesis using a double beam spectrometer (Lambda 650 Perkin-Elmer) from 320 to 720 nm. A quartz cuvette with an optical path length of 10 mm was used for the optical characterization. For reference purposes, the acetone absorption spectrum was recorded. All the experiments were performed under environmental (25 °C and 1 atmosphere pressure) conditions without any special monitoring or control.

2.2.2. Raman characterization

Commercial ZnO powder and the as-obtained ZnO NPs were characterized by Raman microspectroscopy in the rage 250–800 cm^{-1}. A microRaman system (Dimension M1, Lambda Solutions) equipped with a 5 mW CW Nd-YAG (λ = 532 nm) laser and an optical microscope (Olympus BX-41) was used. An objective lens of 50X was utilized to focus down the laser beam on the sample. To perform Raman measurements in the ZnO NPs deposited on glass substrates, samples were prepared by drying at room temperature some drops of the colloidal ZnO NPs suspension on a glass slide. The Raman spectra were captured over 15 acquisitions of 5 s each.

2.2.3. SEM and HRTEM studies

Samples of ZnO NPs deposited on glass substrates were used for the scanning electron microscopy (SEM) characterization. Seemingly, samples for high resolution transmission electron

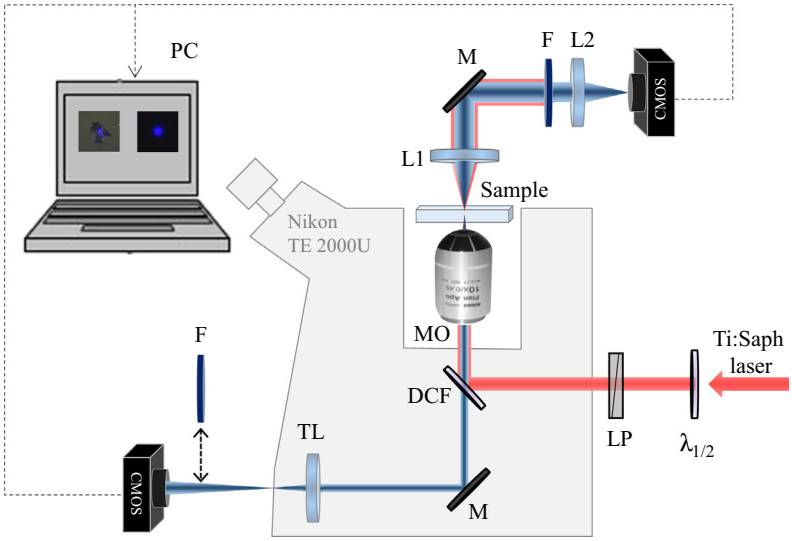

Fig. 2. Optical setup for nonlinear microscopy experiments. $\lambda_{1/2}$: Half Wave-Plate; LP: Linear Polarizer; DCF: Dichroic Filter; MO: Microscope Objective; L1, 2, 3: Condenser, De-scanning and Tube Lens, respectively; M: Mirrors; F: Filter Sets; PC: Personal Computer. CMOS: cameras.

microscopy (HRTEM) characterization were prepared on Cu grids coated with carbon. Through evaporation of the colloidal solution, the ZnO NPs were left behind on the slides/grids. The SEM measurements were carried out using a Scanning Electron Microscope (Hitachi, SU3500) equipment while the HRTEM measurements were carried out using a Transmission Electron Microscope (JEOL 2010), at an accelerating voltage of 200 kV.

2.2.4. Nonlinear optical microscopy experiments

Nonlinear optical microscopy measurements were performed using an ultrashort pulsed laser coupled to an inverted microscope from which the signal is collected in both reflection and transmission modes. The reflection mode is utilized both to image the sample and to collect the backscattered nonlinear signal, while the transmission mode is utilized to characterize the polarization and intensity dependences of the nonlinear process. Fig. 2 depicts the experimental setup viewed from right to left. The incoming ultrashort pulses are generated using a Ti:Sapphire oscillator (TiF-15, AVESTA Ltd.), pumped at 532 nm with a 3 W CW laser (Verdi, Coherent), delivering 820 nm ultrashort 30 fs pulses at a 89 MHz repetition rate and 530 mW of average output power. Prior to enter the inverted microscope (TE 2000 U, Nikon) the laser beam passes through a half-wave plate, $\lambda/2$, which controls the angle of the linearly polarized laser beam. A linear polarizer (LP) can be placed afterwards in the beam path to control the laser power according to the Malus' law. In the microscope system, a short pass dichroic beam splitter, DCF (T750dcspxr, Chroma Tech.), reflects the fundamental laser beam towards the inverted microscope objective, MO (20X, Nikon). The maximum averaged laser power measured after the MO is ~86 mW and the measured lateral resolution of the microscope system is ~2.2 μm (then a radius of 1.1 μm). Therefore, the maximum laser energy fluence delivered at the sample is estimated to be ~26 mJ/cm^2; note that under such laser irradiation conditions no thermal damages of the ZnO NPs are induced [23].

The transmitted nonlinear optical signal is collected at the confocal plane using the telescope system made with the condenser lens, L1, and the de-scanning lens L2. In this plane, the image of the point-spread function is taken using a CMOS color camera (THORLABS DCC1645C) connected to a conventional PC. The fundamental beam is filtered out the beam path to collect only the nonlinear optical signals using different interferometric filter combinations. More specifically, a hot mirror (21001a, Chroma Tech.) and a pass band filter (FF01-420/40; Semrock) combination allows blocking the fundamental 820 nm beam up to 7 orders of magnitude while transmitting 90% between 400 and 440 nm to collect the SHG signal. In the reflection mode, the nonlinear signal is collected with the MO, transmitted through the DCF and, by means of a third lens, L3 (the so-called tube lens), both the sample image and the image of the scattered nonlinear signal at the laser focus are taken simultaneously with a second CMOS camera connected to the PC. Finally, the images taken are processed using ImageJ; an open source image processing package.

3. Results and discussion

3.1. Absorption spectrum of ZnO NPs in acetone

Absorption spectra evolution after synthesizing the ZnO NPs in acetone solution are presented in Fig. 3. The curves are normalized to the absorption spectra of acetone in order to observe the development of the characteristic peak at around 350 nm, which is formed due to ZnO NPs exciton resonance absorption [22]. Note that the peak starts to be appreciated at the 5th day after the NPs synthesis, then it continues evolving throughout the days, and finally it keeps unchanged from the 30th day onwards. In the process, just after the synthesis, a small ZnO shell is formed around Zn NPs core, then the NPs keeps oxidizing towards the Zn core as the time passes by until full oxidation. During this period of time, a decrease in both the absorption peak and broadness of the 351 band is clearly appreciated allowing the transmission of VIS light (>400 nm). As an end result, the solution transparency increases. This transmittance evolution of the colloidal suspension is depicted in the Fig. 3 inset, from day 1 after the synthesis an up to day 30th, passing from dark yellow to a more translucent solution. The corresponding energy band of the measured absorption peak at 351 nm (~3.53 eV) indicates the formation of ZnO NPs below 10 nm in size according to tight binding model calculations [24] and effective mass models used to compute the NPs ZnO radius [25]. Note that no shift of the absorption peak (and so the energy band) is observed. This indicates that the increase of the NPs size during the oxidation process is not considerably affected.

3.2. Raman characterization of ZnO NPs

In Fig. 4 the Raman spectra measured in the 250–800 cm^{-1} range, of the commercial ZnO powder (spectrum (a)) and the as-obtained material (spectrum (b)), are shown. The Raman spectrum corresponding to the commercial powder (bulk ZnO) is constituted by peaks centered at 330, 380, 410, 435, 540, 584 and 662 cm^{-1} [26]. The peak centered at 436 cm^{-1} is the most intense and has its origin in the vibrations of Zn-O in the interior of ZnO crystals, commonly observed in micro-sized particles as it is the case for commercial powders. On the other hand, the spectrum of the as-obtained material presents a photoluminescent background and a wide band centered at 560 cm^{-1} corresponding to the vibrational surface mode that is dominant in the case of ZnO NPs [26,27]. The peak at 435 cm^{-1} has a very low intensity. This result indicates that the obtained material is constituted by ZnO NPs.

3.3. SEM and HRTEM results

Scanning Electron Microscopy (SEM) and High Resolution Transmission Electron Microscopy (HRTEM) were used to assess the NPs morphology at different size scales. In Fig. 5(a) a SEM image displays aggregated ZnO NPs at the micrometer scale. As one can see, granular ZnO is the type of material supported on the glass slide. It is worth noting that the SHG experiments were performed in that kind of sample. On the other hand, in Fig. 5(b) the HRTEM image shows that the clusters are conformed by spheroidal nanoparticles of around 5–8 nm size. The morphology and size of the obtained ZnO NPs are in good agreement with the data from the literature; there exist many reports related to the use of the LASL technique where ZnO NPs have been obtained in several liquid media including water, ethanol, methanol, SDS, acetone. In the most of cases spheroidal ZnO NPs with sizes ranging from 5 to 80 nm were obtained [10,15]. However, it is clear that a more detailed analysis needs to be performed to gain insight of the entire features of the obtained ZnO NPs. Such an analysis is currently underway in view of a better understanding of both isolated and aggregates of the ZnO NPs.

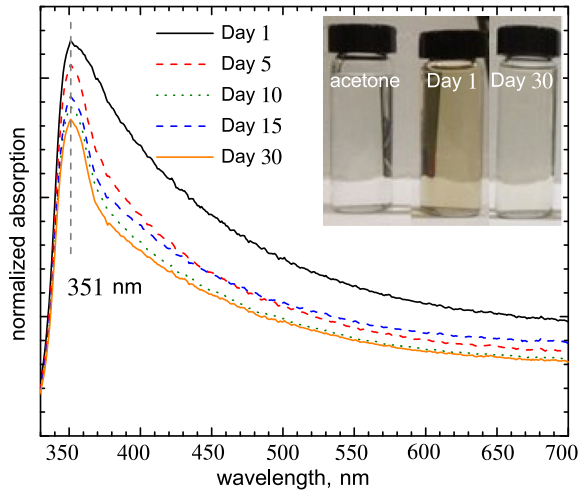

Fig. 3. Normalized absorption spectra of ablated ZnO NPs in acetone taken at different ageing times. The formation evolution of the resonance absorption peak at 351 nm, due to ZnO NPs exciton resonance, is observed. All the spectra are normalized against the absorption spectrum of acetone.

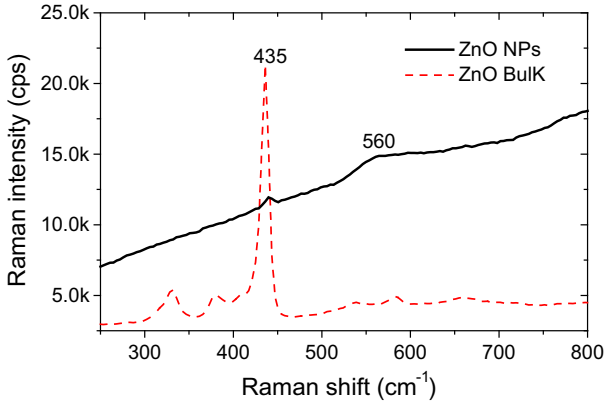

Fig. 4. Raman spectra of ZnO. Commercial ZnO powder (Red line) and the as-obtained ZnO NPs (black line). (For interpretation of the references to colour in this figure legend, the reader is referred to the web version of this article.)

3.4. Second harmonic generation in Zn/ZnO synthesized by LASL

Fig. 6 shows the characterization of the SHG signal originated from the ZnO NPs aggregates shown in Fig. 5(a). The same structures are also appreciated in the bright field image shown in Fig. 6(a), taken through the microscope in reflection mode, where the blue[1] signal corresponds to the back-scattered SHG, which is observable with the naked eye. In contrast to other reports, where a 500 mW pump power was used to observe SHG signal from ZnO NPs [2,4], our system allowed us to observe it at lower powers (below100 mW), and CMOS camera integration times <300 ms. Otherwise, the transmission mode of our microscope system (see Fig. 2) is used to take the SHG image at the confocal plane and it is shown in Fig. 6(b). A set of conveniently chosen band pass filters is used to collect the SHG signal only.

The microscope transmission mode is used to obtain both the intensity and the polarization dependence of the SHG signal by means of the half-wave plate and the linear polarizer as already described above. In Fig. 6(c) and (d) the transmitted SHG signal taken at two different locations within the sample are shown in solid black squares and open gray diamonds, respectively. Note that the dependence of the SHG signal with respect to the laser input power is quadratic (plotted in log-log scale in Fig. 6(c)) due to the 2nd order nonlinearity of the process. However, instead of the expected isotropic polarization dependence of the SHG signal, due to randomly oriented ZnO monocrystalline structures [4,28], both nearly isotropic and well-defined anisotropy dependences were observed in our samples. This is shown in Fig. 6(d) with the open gray diamonds and the solid black squares polar plots, respectively. Note that similar isotropic and anisotropic SHG signal dependences were obtained throughout the sample and for different ZnO NPs samples obtained under similar synthesis conditions (data not shown).

While the origin of the isotropic SHG signal is attributed to randomly organized monocrystalline ZnO NPs, the anisotropic SHG could be originated from aggregated NPs forming ZnO microstructures. Note that, in either case, the signal is visible to the naked eye as reported in previous work performed on larger ZnO NPs [1–7]. This suggests that the high efficiency of the SHG process in ZnO NPs may not depend on the nanoparticles size or the aggregation state. Our hypothesis is supported with results published just recently by Multian et. al., where it is found that the SHG signal from 2 nm ZnO NPs suspensions is comparable to the SHG signal obtained from commercial 150 nm ZnO NPs suspensions [12].

In this sense, knowing the origin of the SHG efficiency with respect the NPs size, would be important to estimate the limits

[1] For interpretation of color in Fig. 6, the reader is referred to the web version of this article.

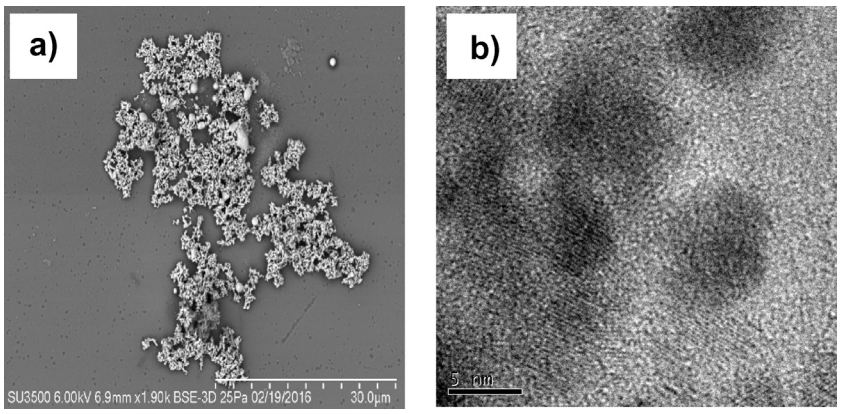

Fig. 5. Morphology of synthesized ZnO NPs. (a) SEM image of the ZnO NPs deposited on a glass slide. (b) HRTEM image of ZnO NPs clusters conformed of spheroidal nanoparticles of around 5–8 nm size.

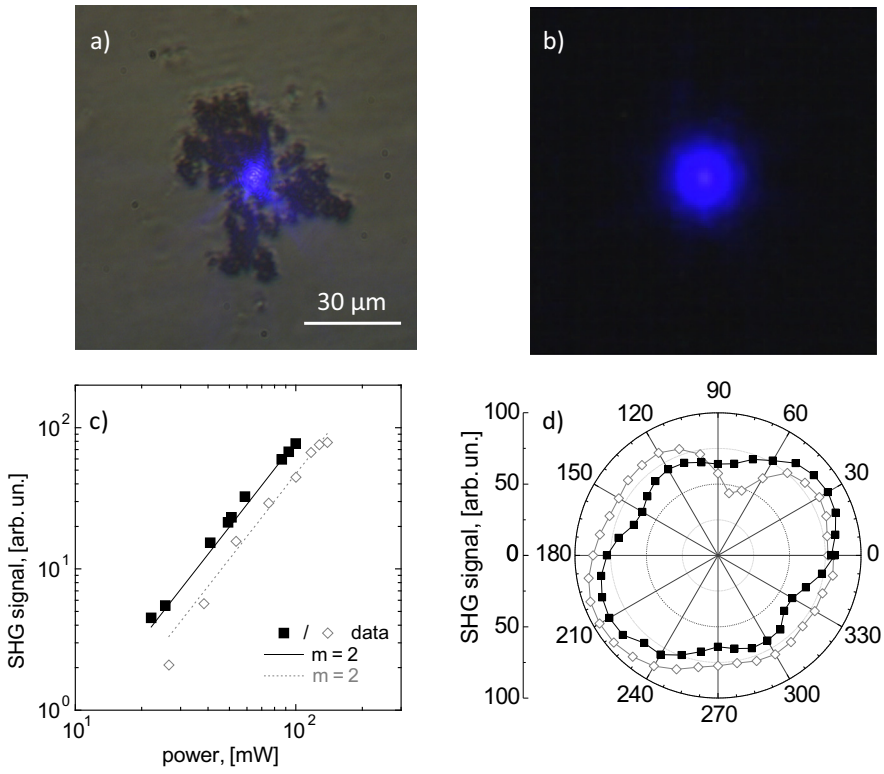

Fig. 6. Characterization of SHG signal in ZnO synthetized by LASL. (a) Bright file mage of clustered ZnO nanoparticles showing simultaneously the back scattered SHG signal at the laser focus taken in the reflation mode; (b) image of the SHG signal at the confocal plane taken in the transmission mode. (c) Log-log scale plots showing the typical quadratic SHG signal dependence with respect the laser input power (see fitted curves with slopes m = 2) due to a 2nd order optical nonlinear process; and d) polar plot showing the polarization dependence of SHG signal. Figures (c) and (d) shows the results taken at two different location with the sample.

of the nonlinear optical process. Therefore, we believe that more studies in this direction are foreseen. Additionally, the optimum size of ZnO NPs also needs to be investigated in view of using these NPs as bio-markers for cell imaging. This taking into consideration that the optimum size for nanoparticles cellular uptake (endocytosis) in living cells is estimated to be between 30 and 50 nm [29,30], and also considering that cell cytotoxicity increases for smaller NPs sizes [31,32].

4. Conclusions

We reported the use of LASL technique for the facile and fast synthesis of ZnO NPs with second order nonlinear optical properties (SHG). The ZnO NPs showed the characteristic sharp resonance absorption peak at 351 nm due to ZnO nanoparticles exciton resonance absorption. Analysis by HRTEM showed ZnO NPs with average nanoparticle size of 5–8 nm. Efficient SHG signal from aggregated ZnO NPs, containing small sized nanoparticles, is observed. While nearly isotropic SHG signal is attributed to randomly distributed ZnO monocrystalline NPs, anisotropic SHG could be originated from aggregated form of the ZnO NPs microstructures. The comparable signals suggest that the SHG efficiency may not depend on the NPs size or aggregation state. A more detailed study to determine the origin of the SHG efficiency of smaller ZnO NPs is required. LASL technique is an experimentally simple technique to synthesize in a controlled manner

biocompatible nanoparticles, which represent a cost effective and green alternative way of designing potentially efficient biomarkers for nonlinear imaging applications.

Acknowledgments

This work was partially supported by SIEA-UAEMex under the contracts 3798/2014/CID and 3885/2015FS, CONACYT through grant 251992 and AFOSR through grant FA9550-15-1-0142. YLP acknowledges to CONACYT for financial support through grant 628904 to develop her master studies within the Programa de Posgrado en Ciencia de Materiales de la UAEMex. Finally, we acknowledge CCIQS-UAEM-UNAM for making their TEM facilities available. GA and SCL would like to acknowledge the partial financial support of NSF grant 1545852 (OISE:PIRE-SOMBRERO)/ CONACyT 251992 and GA also acknowledges the support of NSF grant 1547014 (DMR:EAGER).

Author contributions

SCL, MCL and GA supervised the project as the scientific group leaders and principal investigators. MACL and MCL conceived the idea of using LASL technique for the ZnO NPs synthesis. IRM, SCL and MACL conceived the idea of studying the nonlinear SHG properties of the synthetized NPs. YLP and YEB performed the SHG measurements. YLP performed the absorption and electron microscopy measurements. YPL and IRM performed the data analysis. All the authors analyzed and discussed the results. All authors contribute in the manuscript writing. All authors read and approved the final manuscript.

Competing interests

The authors declare that they have no competing interests.

References

[1] N.S. Han, H.S. Shim, S.M. Park, J.K. Song, Second-harmonic generation and multiphoton induced photoluminescence in ZnO, Bull. Korean Chem. Soc. 30 (10) (2009) 2199–2200.
[2] B.E. Urban, J. Lin, O. Kumar, K. Senthilkumar, Y. Fujita, A. Neogi, Optimizaton of nonlinear optical properties of ZnO micro and nanocrystals for biophotonics, Opt. Mater. Exp. 1 (4) (2011) 658–669.
[3] B.E. Urban, P. Neogi, K. Senthilkumar, S.K. Rajpurohit, P. Jagadeeshwaran, S. Kim, A. Neogi, Bioimaging using the optimized nonlinear optical properties of ZnO nanoparticles, IEE J. Sel. Topics Quantum Electron. 18 (4) (2012) 1451–1456.
[4] B. Christopher, B. Nelson, K.E. Shane, A.A. Al-Nossiff, S. Mahamud, Optical second harmonic generation from ZnO nanofluids – a tight binding approach in determining bulk $\chi^{(2)}$, J. Phys. Chem 119 (2015) 2630–2636.
[5] K. Pedersen, C. Fisker, T.G. Pedersen, Second-harmonic generation from ZnO nanowires, Phys. Status Solidi C 5 (8) (2008) 2671–2674.
[6] E. De la Rosa, M. Yacaman, L. Sun, M.C. Downer, L.A.D. Torres, P. Salas, Second-harmonic imaging of ZnO nanoparticles, in: IEE Lasers and Electro-Optics Conference, 2007, pp. 1–2.
[7] J. Lin, Y. Fujita, A. Neogi, Saturation of two photon emission in ZnO nanoparticles with second order nonlinearity, RSC Adv. 5 (15) (2015) 10921–10926.
[8] J. Ebothe, R. Miedzinski, V. Kapustianyk, B. Turko, B. Kulyk, W. Gruhn, I.V. Kityk, Optical SHG for ZnO films with different morphology stimulated by UV-laser thermotreatment, J. Phys. Conf. Ser. 79 (2007) 012001.
[9] B. Kulyk, B. Sahraoui, O. Krupka, V. Kapustianyk, V. Rudyk, E. Berdowska, S. Tkaczyk, I. Kityk, Linear and nonlinear optical properties of ZnO/PMMA nanocomposite films, J. App. Phys. 106 (9) (2006) 09310.
[10] H. Zeng, X.W. Du, S.C. Singh, S.A. Kulinich, S. Yang, J. He, W. Cai, Nanomaterials via laser ablation/irradiation in liquid: a review, Adv. Funct. Mater. 22 (7) (2012) 1333–1353.
[11] M.H. Mahdieh, B. Fattahi, Size properties of colloidal nanoparticles produced by nanosecond pulsed laser ablation and studying the effects of liquid medium and laser fluence, Appl. Surf. Sci. 329 (2015) 47.
[12] V.V. Multian, A.V. Uklein, A.N. Zaderko, V.O. Kozhanov, O.Y. Boldyrieva, R.P. Linnik, V.Y. Gayvoronsky, Synthesis, characterization, luminescent and nonlinear optical responses of nanosized ZnO, Nanoscale Res. Lett. 12 (1) (2017) 164.
[13] X.Q. Zhang, Z.K. Tang, M. Kawasaki, A. Ohtomo, H. Koinuma, Resonant exciton second-harmonic generation in self-assembled ZnO microcrystallite thin films, J. Phys. Condens. Matter 15 (2003) 5191–5196.
[14] M. Lafrentz, D. Brunne, A.V. Rodina, V.V. Pavlov, R.V. Pisarev, D.R. Yakovlev, A. Bakin, M.B. Nayer, Second harmonic generation spectroscopy of excitions in ZnO, Phys. Rev. 88 (23) (2013) 235207.
[15] A. Kolodziejezak-Radzimska, T. Jesionowski, Zinc oxide-from synthesis to application: a review, Materials 7 (2014) 2833–2881.
[16] A. Amendola, M. Meneghetti, Laser ablation synthesis in solution and size manipulation of noble metal nanoparticles, Phys. Chem. Chem. Phys. 11 (2009) 3805–3821.
[17] M.A. Gondal, Q.A. Drmosh, Z.H. Yamani, T.A. Saleh, Synthesis of ZnO_2 nanoparticles by laser ablation and their annealing transformation into ZnO nanoparticles, Appl. Surf. Sci. 256 (2009) 298–304.
[18] P. Bindu, S. Thomas, Estimation of lattice strain in ZnO nanoparticles: X-ray peak profile analysis, J. Theor. Appl. Phys. 8 (4) (2014) 123–134.
[19] H.E. Palma-Palma, M. Camacho-López, M.A. Camacho-López, A.R. Vilchis-Néstor, Preparation of zinc peroxide nanoparticles by laser ablation of solid in liquids, Sup. y Vac. 28 (3) (2015) 74–77.
[20] K.K. Kim, D. Kim, S.K. Kim, S.M. Park, J.K. Song, Formation of ZnO nanoparticles by laser ablation in neat water, Chem. Phys. Lett. 511 (1) (2011) 116–120.
[21] M.P. Navas, R.K. Soni, Optical properties of laser ablated Zn@ZnO in water, ethanol and methanol, in: International Conference on Condensed Matter and Applied Physics (ICC 2015), AIP Conf. Proc., p. 1728.
[22] D. Dorranian, A.F. Eskandari, Effect of laser fluence on the characteristics of ZnO nanoparticles produced by laser ablation in acetone, Mol. Cryst. Liq. Cryst. 607 (1) (2015) 1–12.
[23] J. Hermann, M. Benfarah, G. Coustillier, S. Bruneau, E. Axente, J.F. Guillemoles, M. Sentis, P. Alloncle, T. Itina, Selective ablation of thin films with short and ultrashort laser pulses, App. Surf. Sci. 252 (13) (2006) 4814–4818.
[24] E.G. Goh, X. Xu, P.G. McCormick, Effect of particle size on the UV absorbance of zinc oxide nanoparticles, Scripta Mater. 78 (2014) 49–52.
[25] S. Talam, S.R. Karumuri, N. Gunnam, Synthesis, characterization, and spectroscopic properties of ZnO nanoparticles, ISRN Nanotech. 2012 (2012) 372505.
[26] H. Zeng, X. Ning, X. Li, An insight into defect relaxation in metastable ZnO reflected by a unique luminescence and Raman evolutions, Phys. Chem. Chem. Phys. 17 (29) (2015) 19637–19642.
[27] H. Zeng, G. Duan, Y. Li, S. Yang, X. Xu, W. Cai, Blue luminescence of ZnO nanoparticles based on non-equilibrium processes: defect origins and emission controls, Adv. Funct. Mater. 20 (4) (2010) 561–572.
[28] E.Y. Morozov, A.A. Kaminskii, A.S. Chirkin, D.B. Yusupov, Second optical harmonic generation in nonlinear crystals with a disordered domain structure, J. Exp. Theor. Phys. Lett. 73 (12) (2001) 647–650.
[29] S. Zhang, J. Li, G. Lykotrafitis, G. Bao, S. Suresh, Size-dependent endocytosis of nanoparticles, Adv. Mater. 21 (4) (2009) 419–424.
[30] L. Shang, K. Nienhaus, G.U. Nienhaus, Engineered nanoparticles interacting with cells: size matters, J. Nanobiotech 12 (5) (2014).
[31] J.W. Rasmussen, E. Martinez, P. Louka, D.G. Wingett, Zinc oxide nanoparticles for selective destruction of tumor cells and potential for drug delivery applications, Expert Op. Drug Deliv. 7 (9) (2010) 1063–1077.
[32] C. Hanley, A. Thurber, C. Hanna, A. Punnoose, J. Zhang, D.G. Wingett, The influences of cell type and ZnO nanoparticle size on immune cell cytotoxicity and cytokine induction, Nanoscale Res. Lett. 4 (12) (2009) 1409.